Inhibiting fibronectin assembly in the breast tumor microenvironment increases cell death and improves response to doxorubicin

Metti K. Gari[1], Hye Jin Lee[2], David R. Inman[1], Brian M. Burkel[1], Margaret A. Highland[3], Glen S. Kwon[4], Nikesh Gupta[4], and Suzanne M. Ponik[1*]

[1] Department of Cell and Regenerative Biology, University of Wisconsin-Madison, Madison, WI, USA

[2]College of Pharmacy, Chungbuk National University, Cheongju 28160, Republic of Korea

[3] Wisconsin Veterinary Diagnostic Laboratory, University of Wisconsin - Madison, WI, USA

[4]Pharmaceutical Sciences Division, School of Pharmacy, University of Wisconsin - Madison, WI, USA

[5]Carbone Cancer Center, University of Wisconsin - Madison, Madison, WI, USA

*Corresponding Author: ponik@wisc.edu

Abstract

Purpose: Effective therapies for solid tumors, including breast cancers, are hindered by several roadblocks that can be largely attributed to the fibrotic extracellular matrix (ECM). Fibronectin (FN) is a highly upregulated ECM component in the fibrotic tumor stroma and is associated with poor patient prognosis. This study aimed to investigate the therapeutic potential of an anti-fibrotic peptide that specifically targets FN and blocks the fibrillar assembly of FN.

Methods: To target FN, we used PEGylated Functional Upstream Domain (PEG-FUD), which binds to the 70 kDa N-terminal region of FN with high affinity, localizes to mammary tumors, and potently inhibits FN assembly in vitro and in vivo. Here, we used the 4T1 tumor model to investigate the efficacy and mechanisms of PEG-FUD to inhibit tumor growth.

Results: Our data demonstrates that PEG-FUD monotherapy reduces tumor growth without systemic toxicity. Analysis of the tumor microenvironment revealed that PEG-FUD effectively inhibited FN matrix assembly within tumors and reduced adhesion-mediated signaling through α5 integrin and FAK leading to enhanced tumor cell death. Notably, signaling through FAK has been associated with resistance mechanisms to doxorubicin (DOX). Therefore, we tested the combination of PEG-FUD and Dox, which significantly reduced tumor growth by 60% compared to vehicle control and 30% compared to Dox monotherapy.

Conclusions: Our findings demonstrate that PEG-FUD significantly modifies the peritumoral ECM of breast cancer, leading to increased tumor cell death, and potentiates the efficacy of conventional breast cancer therapy.

Keywords: Fibronectin, tumor microenvironment, adhesion signaling, breast cancer therapy, Doxorubicin

Introduction

Therapies for solid tumors, including breast cancer, are hindered by several roadblocks that can be largely attributed to the fibrotic ECM in the microenvironment of these tumors. The fibrotic ECM in the breast tumor microenvironment (TME) is well-known for promoting tumor aggressiveness, metastatic progression, and mechanisms of therapy resistance(1–3). During tumor progression, the deposition of ECM proteins such as collagen and FN is significantly increased, which results in tumor fibrosis. Importantly, the excess deposition of ECM in the breast TME along with alterations in ECM architecture are associated with poor breast cancer patient outcome(4–9). Based on the abundance of ECM in solid tumors and the importance of the fibrotic ECM in breast cancer

progression, multiple efforts have been made to therapeutically target the ECM. To date, ECM targeting strategies have focused on interfering with ECM-modulating enzymes or signaling pathways involved in the deposition, degradation, and remodeling of ECM components (10–13). Despite the promising pre-clinical success of existing ECM-targeting drugs, most fail to transition to the clinic due to toxicity and off-target effects(14–17). Hence, there is a need to develop new therapies that specifically target the ECM and are potent enough to achieve efficacy while maintaining safety.

In this study, we focus on directly targeting FN, one of the major ECM proteins identified in the fibrotic tumor matrix(18–20). FN is a multifunctional glycoprotein that exists in two major forms, plasma FN secreted from the liver and cellular FN that is secreted locally by various cell types (21). Despite the source, FN is secreted as a soluble dimer in a compact inactive state, where it can be incorporated into an insoluble fibrillar matrix upon binding to cell surface receptors, including the integrin receptor α5β1(22). The N-terminal 70-kDa region of FN is required for the assembly of FN into an insoluble fibrillar matrix(23). Insoluble or assembled FN matrix in the TME plays a crucial role in scaffolding other ECM proteins, stabilizing the ECM, and providing adhesion sites to initiate tumor cell signaling cascades that enhance proliferation and viability(24–26). To specifically target FN and block the fibrillar assembly of FN, we chose to use the small 6-kDa bacterial-derived peptide called Functional Upstream Domain (FUD/pUR4) discovered by Tomasini-Johansson et al(27). FUD binds to the N-terminal 70-kDa region of both sources of FN (cellular and plasma) with nanomolar binding affinity, consequently, blocking the extension of FN and assembly into fibrils(27). Importantly, FUD is a potent inhibitor of FN assembly both *in vitro* and *in vivo*(28–30). Several laboratories have demonstrated the potential of FUD as a therapeutic agent in multiple fibrotic diseases, including breast cancer(31). However, the peptide is rapidly

70 cleared through the renal system, which limits the *in vivo* bioavailability and results in daily
71 required FUD administration at a relatively high dose of ~25 mg/kg(32). To address the issue of
72 rapid renal clearance, we PEGylated-FUD (PEG-FUD) and demonstrated a significant increase in
73 peptide bioavailability and tumor retention compared to non-PEGylated FUD, while maintaining
74 the ability to inhibit FN assembly(33–36).

75 Here, we investigated the anti-cancer efficacy of PEG-FUD in the TNBC 4T1 mouse mammary
76 carcinoma model. We hypothesized that modulating FN assembly into a fibrillar matrix with PEG-
77 FUD would disrupt cell-ECM interactions thereby inhibiting tumor growth, blocking mechanisms
78 of drug resistance, and improving the efficacy of chemotherapy. Our study revealed that treatment
79 with PEG-FUD significantly decreased 4T1 tumor growth. By characterizing the alterations in the
80 TME in response to PEG-FUD, we identified a significant inhibition of FN matrix assembly,
81 reduced levels of cell adhesion proteins (including α5 integrin and FAK), and an increase in
82 caspase-3 mediated cell death. Further investigation into the potential of PEG-FUD to improve
83 chemotherapy response revealed that co-treatment with PEG-FUD significantly enhanced the anti-
84 tumor efficacy of Dox without any additional systemic toxicity.

85

86 Materials and Methods

87 Preparation of Functional Upstream Domain (FUD) peptide and its mutated counterparts

88 FUD and the FUD control (mutated FUD (mFUD) and Fully mutated FUD (FmFUD)) constructs
89 were a kind gift from Dr. Donna Peters at University of Wisconsin-Madison. The mFUD and
90 FmFUD control peptides have reduced binding affinity for FN due to point mutations in the FN
91 binding regions. All peptide sequences were cloned into the pET-ELMER vector and

recombinantly expressed in BL21 *Escherichia coli* (DE3) as His-tagged peptides as previously described by our group(33–36). Briefly, 1 mM of isopropyl β-D-1thiogalactopyranoside (IPTG) was added to the obtained 1L culture to induce expression of FUD/mFUD/FmFUD. The resulting bacterial pellet was suspended in the lysis buffer (pH 8.0) [Urea 8M, NaH_2PO_4 100 mM, Tris 10 mM, Imidazole 5 mM] and centrifuged to obtain clear supernatant. Ni-NTA agarose (Qiagen) beads were equilibrated with the lysis buffer and 1 mL of Ni-NTA agarose resin was added for every 4 mL of the above obtained lysate and incubated overnight at 4°C with Ni-NTA agarose beads. The next day, the lysate was removed and the Ni-NTA agarose was washed with a washing buffer (pH 8.0) [Urea 8M, NaH_2PO_4 100 mM, Tris 10 mM, Imidazole 15 mM] and equilibrated with Thrombin cleavage buffer (pH 8.4) [$CaCl_2$ 2.5 mM, NaCl 150 mM, Tris 20 mM]. Elution of peptides and removal of the His tag was achieved by using a thrombin cleavage site between the His-tag and the corresponding peptide (FUD/mFUD/FmFUD). FUD bound to the Ni-NTA agarose was incubated with ~36 units of Bovine α-Thrombin for every 15 mL of sample. The eluted sample was collected and further purified via fast protein liquid chromatography (FPLC) using HiTrap Q HP column from Cytiva.

PEGylation of FPLC purified peptides

PEGylated conjugates were synthesized using reductive amination chemistry. FUD, mFUD or FmFUD peptide(s) were N-terminally selectively conjugated with 20-kDa methoxy-PEG-propionaldehyde using the previously published protocol by our group(33). Briefly, the FPLC purified FUD/mFUD/FmFUD peptide was mixed with PEG in a sodium acetate buffer solution (50 mM, pH 5.5) in the presence of $NaBH_3CN$ and the reaction was carried out for ~18 hr in the fuming cabinet under cold conditions (4°C). After the reaction time was complete, the mixture was

115 dialyzed two times against NaOAc buffer to remove excess reducing agent. Next, the buffer was
116 switched to 20mM Tris and left overnight before FPLC purification via ion-exchange
117 chromatography using 5mL HiTrap Q HP anion exchange column. The concentration of
118 FUD/mFUD/FmFUD was obtained by measuring the absorbance at 280 nm using corresponding
119 ε values [0.496 (FUD), 0.742 (mFUD) and 0.250 (FmFUD)]. Patent number for PEG-FUD:
120 US10828372B2.

121

122 **Enzyme-linked competition binding assay**

123 The enzyme-linked competition binding assay was carried out as previously reported(37,38), with
124 a small modification. Briefly, a 96-well high-binding culture plate was coated overnight with
125 human plasma FN under cold conditions (4°C) at 10 μg/mL of concentration. The biotinylated
126 FUD (b-FUD) was prepared as per the manufacturer's protocol using NHS-biotin-ester (Pierce).
127 The above FN-coated plate was blocked for 1 hr using 5% BSA prepared in tris-buffered saline
128 containing 0.05% Tween 20 (TBS-T). 0.5 nM of b-FUD was added to the plate concurrently with
129 various concentration (2000, 1000, 500, 250, 125, 62.5, 0 nM) of unlabeled PEG-FmFUD or PEG-
130 FUD in 0.1% BSA in TBS-T. After a 2 hr incubation at RT, followed by three TBS-T washes,
131 alkaline phosphatase-conjugated streptavidin (Jackson Immunoresearch) was added at 1:20,000
132 dilution factor and incubated for 1 hr at RT. After washing with TBS-T again, 100 uL of 1-step p-
133 Nitrophenyl Phosphate was added as a substrate to each treated well, and the reaction was stopped
134 by the addition of 2N sodium hydroxide. Absorbance was measured at 405 nm using a microplate
135 reader.

136

137 **Cell monolayer culture**

138 4T1 breast cancer cells were obtained from American Type Culture Collection (VA). 4T1 cells
139 were cultured in Rosewell Park Memorial Institute Medium-1640 (RPMI) (Corning, NY, USA)
140 containing 10% fetal bovine serum (FBS). The human breast cancer-associated fibroblasts
141 (hCAFs) cells were a gift from Charlotte Kupperwaser's laboratory at Tufts University. The hCAFs
142 were cultured in Dulbecco's Modified Eagle Medium (DMEM, Gibco) containing 10% FBS and
143 1% streptomycin/penicillin. The bone-marrow-derived fibroblast cells isolated from the femurs of
144 BALB/c mice were cultured in DMEM containing 20% FBS and 1% streptomycin/penicillin and
145 activated by 4T1-conditioned media to generate murine cancer-associated fibroblasts (mCAFs) as
146 described previously (39). All cell cultures were kept at 37°C in the humidified incubator with 5%
147 CO_2. For tumor cell inoculations, cells were washed, harvested and counted manually using a
148 hemocytometer.

149

150 **Cell monolayer ECM staining**

151 To confirm ECM changes in fibroblast culture after PEG-FUD incubation, 25,000 hCAFs or
152 mCAFs in corresponding media containing 50 μg/ml of ascorbic acid were seeded onto a 35 mm
153 glass bottom dish (VWR). The next day, 250 nM of PEG-FUD peptides in phosphate-buffered
154 saline (PBS) were incubated with hCAFs or 500 nM of PEG-FUD was incubated with mCAFs for
155 48 hr. PBS was used as a vehicle in control groups. After the peptide incubation, cells were washed
156 with Hanks' Balanced Salt Solution and fixed with 10% formalin for 10 min at RT. Following
157 fixation, 2% BSA in PBS was used for blocking for 1 hr at RT. hCAFs were incubated with a
158 A488-labeled anti-FN primary antibody (eBioscience, No. 53-9869-82, 1:100) in 1% BSA/PBS at

159 4°C overnight. The next day, cells were washed to remove unbound primary antibody. mCAFs,
160 were immunolabeled using a rabbit anti-mouse FN primary antibody (1:500) (34) in 1% BSA/PBS
161 at 4°C overnight and an A488-labeled goat anti-rabbit (Life technologies, A11034, 1:500)
162 secondary antibody in 1% BSA in PBS for 1 hr at RT. After washing, nuclei were stained with
163 DAPI (D9542, MilliporeSigma). Confocal microscopy (Nikon AIRS with 20x objective lens) was
164 used to visualize the assembled FN by the fibroblasts, and images were processed with the vendor
165 software (NIS-Elements).

166

167 **Animal Tumor model**

168 9-week-old female BALB/c mice were purchased from Jackson Labs and housed in the Wisconsin
169 Institutes for Medical Research animal facilities at the University of Wisconsin-Madison. All
170 experiments were conducted in compliance with the University of Wisconsin Institutional Animal
171 Care and Use Committee (IACUC). 4T1 tumors were established by orthotopically injecting 2×10^5
172 4T1 cells in 50 µl DPBS into the fourth mammary fat pad of syngeneic, immunocompetent
173 BALB/c mice. To minimize tumor abrasion, mice were housed on soft bedding. To assess FN
174 protein levels, major organs such as the mammary glands, lungs, liver, spleen, and kidney were
175 harvested from 4T1 tumor bearing and non-tumor bearing control mice 4 weeks after 4T1 cell
176 inoculation. For PEG-FUD monotherapy, after orthotopic tumor injection, all mice were randomly
177 assigned to an experimental group. After 1 week of tumor growth, when tumor size reached
178 approximately 50 mm^3, vehicle control (Ctrl_PBS) or peptides (PEG-FmFUD, PEG-mFUD and
179 PEG-FUD) were administered subcutaneously at the scruff of the neck every 48 hr at a dose of
180 12.5mg/kg (outlined in Fig 3). For combination therapy (PEG-FUD + Dox), 4 doses of PEG-FUD
181 or control peptides were administered every 48 hrs, then Dox treatment was initiated, which

182 consisted of intraperitoneal administration every 72 hr at 5 mg/kg along with continued peptide
183 dosing every 48 hrs (outlined in Fig 7A). During the treatment course, tumor growth was measured
184 manually every 48 hr using a caliper, starting at the first treatment. Tumor volume was calculated
185 using the formula $V = ½ (Length \times Width^2)$(40). The maximal tumor volume approved by the
186 IACUC at the University of Wisconsin-Madison is 1.5 cm^3. In compliance with these guidelines,
187 all animals in this study were euthanized at or before tumors reached this volume (Supplemental
188 Table 1A-B). At the end of the treatment, blood was collected, mice were euthanized, and tissues
189 were harvested for subsequent analysis.
190
191 **Toxicity evaluation**
192 Body weight was monitored every 48 hr during the treatment course. At the experimental end
193 point, blood was collected via cardiac puncture to perform a complete blood count (CBC) analysis
194 using the VETSCAN® HM5 Hematology Analyzer. During harvest, the spleen was collected and
195 weighed. Additionally, kidneys and liver were harvested and fixed in 10% buffered formalin for
196 48 hr at 4 °C. Fixed tissues were paraffin embedded and 5 µm sections were stained with
197 hematoxylin and eosin (H&E) by routine methods. Stained slide sections were captured at 40x by
198 Aperio Digital Pathology Slide Scanner system and the digitized slides were evaluated by a board
199 certified veterinary anatomic pathologist using Aperio ImageScope [v12.4.6.5003].
200
201 **Immunofluorescence staining**
202 4T1 tumors were fixed for 48 hr at 4 °C in 10% buffered formalin. Fixed tissues were paraffin-
203 embedded and sectioned into 5 µm sections for immunofluorescence analysis. Briefly, tissue
204 sections were deparaffinized in a humidity chamber with xylene and rehydrated in graded ethanol

205 washes. Next tissue sections were subjected to heat-induced antigen retrieval in citrate buffer pH
206 6.0. Slides were blocked with 10% BSA in TBS for 1 hr then incubated for 1 hr at RT with primary
207 antibodies, FN (ab23750, Abcam, 1:250) and Antigen Kiel 67- Ki67 (ab15580, Abcam, 1:100),
208 followed by washing in TBS-T. Next, samples were incubated with secondary antibody (ab7090,
209 Abcam, 1:500) for 10 min at RT. For amplified fluorescence detection, sections were incubated
210 with TSA substrates (PerkinElmer) for 10 min at RT, followed by nuclear counterstaining with
211 DAPI (D9542, MilliporeSigma). Slides were coverslipped using ProLong Gold (no. P36930;
212 Thermofisher). Immunofluorescent labeled slides were imaged using a Leica Thunder imaging
213 system with 10x magnification. Quantification of >10 fields of view was performed in Image J for
214 each staining.
215
216 **Picro-sirius red (PSR) staining**
217 Formalin fixed paraffin embedded (FFPE) 4T1 tumor tissues were sectioned at 5 μm for PSR
218 staining. Briefly, tissue sections were deparaffinized with xylene and underwent sequential washes
219 of graded ethanol as described above. Next slides were stained with PSR (Sigma-Aldrich; "Direct
220 Red 80"; Catalog # 36-554-8) for 1 hr. Slides were then washed with acidified water, dehydrated
221 in 100 % ethanol, and cleared in xylene. Slides were coverslipped using Richard-Allan Scientific
222 Mounting Medium (REF 4112, Thermo Scientific). PSR stained slides were imaged at an
223 excitation wavelength of 575 nm using Leica Thunder imaging system with a magnification of
224 20x. Quantification of >10 fields of view were performed in Image J.
225
226 **TUNEL staining**

227 FFPE 4T1 tumor sections were deparaffinized and rehydrated as described above. Sections were
228 then stained with a 1:10 dilution of TUNEL enzyme in TUNEL buffer (Roche In Situ Cell
229 Detection Kit w/Fluorescein. Catalog # 11684795910) for 1 hr at 37°C, washed with PBST, and
230 coverslipped with ProLong Gold mounting media (no. P36930; Thermofisher). TUNEL stained
231 slides were imaged at an excitation wavelength of 475 nm using Leica Thunder imaging system
232 with a magnification of 20x.
233
234 **Western Blotting**
235 Tissues were fractionated into soluble and insoluble lysates similar to our prior study(34). Briefly,
236 tissues were cryopulverized using a mortar and pestle in the presence of liquid nitrogen. The
237 homogenized samples were lysed in RIPA buffer containing 1% deoxycholate (DOC) at 0.1 g
238 tissue per ml buffer and spun at 4°C. The supernatant was collected, and the pellets were
239 solubilized in buffer containing 4 M urea, 4% SDS and 1 mM DTT. Resuspended pellets were
240 vortexed, sonicated, and heated to 95°C for 5 min. The DOC-soluble supernatant contains nuclear,
241 cytoplasmic, and membrane fractions, while mainly ECM proteins constitute the DOC-insoluble
242 pellet. Protein concentrations were measured using the DC Protein Assay kit (Bio-Rad) and BSA
243 standards, diluted in the corresponding buffers. Proteins in each fraction were separated by SDS–
244 polyacrylamide gel electrophoresis and transferred to a polyvinylidene difluoride membrane. To
245 ensure even protein loading and transfer efficiency, total protein (TP) staining (Fast Green FCF,
246 MilliporeSigma) was performed. Next, membrane was blocked with 5% non-fat dry milk solution
247 in TBS-T, and incubated overnight at 4°C with the following primary antibodies: FN (ab23750,
248 Abcam, 1:250, 2hr); COL1A1 (NBP1-30054, Novus Biologicals, 1:500); tenascin-C (ab108930,
249 Abcam, 1:500); periostin (ab14041, Abcam, 1:500) ; proliferating cell nuclear antigen - PCNA

250 (#13110, Cell Signaling, 1:500); Caspase-3 (#9662, Cell Signaling, 1:500); integrin α5 (10569-1-
251 AP, proteintech, 1:1000); integrin β1 (#34971, Cell Signaling, 1:1000); FAK (#05-537,
252 MilliporeSigma, 1:1000). Proteins were detected using either a horseradish peroxidase–conjugated
253 secondary antibodies (Jackson ImmunoResearch) followed by chemiluminescence substrate (LI-
254 COR BioScience) or fluorescent–conjugated secondary antibodies (IRDye infrared dyes from LI-
255 COR Biosciences). Blots were imaged using the Odyssey Fc Imager and band intensities were
256 analyzed using Image studio. For detection of plasma FN, blood was isolated from mice via cardiac
257 puncture and spun for 10 min at 2,000 x-g to remove cells. Next, the plasma layer was collected
258 and spun for 15 min at 2,000 x-g to deplete platelets in the plasma. The supernatant was collected
259 and put in 2x Laemmli followed by standard procedures of Western blotting as described above.
260

261 **Statistics**

262 GraphPad Prism was used to generate graphs and perform statistical analysis. For comparison
263 between two groups, an unpaired t-test was performed. For comparison between multiple groups,
264 a one-way analysis of variance (ANOVA) with Tukey's Multiple Comparison Test (TMCT) was
265 performed, with a corrected P value ≤ 0.05 considered significant. Data is reported as mean ± s.e.m.
266

267 ## Results

268 **PEG-FUD inhibits mammary CAF-mediated FN assembly *in vitro***

269 Cancer-associated fibroblasts (CAF) are one of the most abundant stromal cells in the TME and
270 the primary cell type responsible for the deposition of ECM proteins, including FN. CAFs not only
271 secret FN but also assemble FN(41). We previously showed that Cy5-labeled PEG-FUD can bind
272 to exogenous or endogenous FN assembled by CAFs(36). Prior studies have shown that PEG-FUD

273 inhibits FN assembly by human foreskin fibroblasts(33,42), however, PEG-FUD has yet to be
274 demonstrated as an inhibitor of FN assembly by mammary CAFs. To confirm PEG-FUD inhibits
275 mammary CAF-mediated FN matrix assembly, we induced ECM matrix assembly in hCAFs or
276 activated mCAFs and treated cells with control (Ctrl_PBS) or PEG-FUD (250 or 500 nM,
277 respectively) for 48 hrs. At experimental endpoint, the cultures were fixed and the fibrillar structure
278 of FN was visualized by immunofluorescence staining. PEG-FUD significantly decreased the area
279 of cellular FN assembled by mCAFs (Fig 1A-B). Additionally, we identified a similar decrease in
280 hCAF-mediated fibrillar FN assembly in the presence of PEG-FUD compared to the control, PBS-

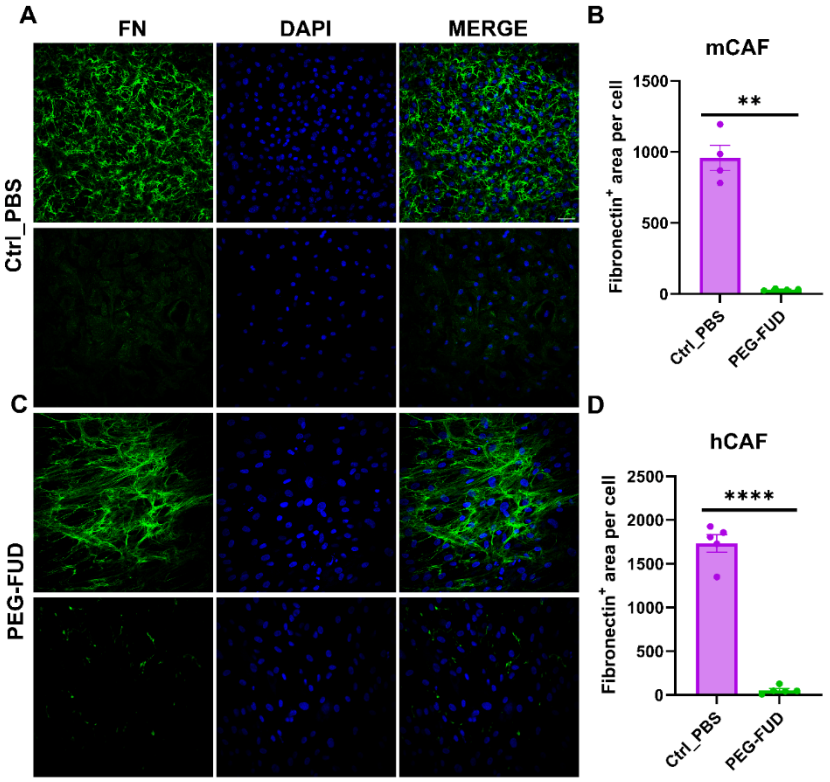

Figure 1: **Fibronectin (FN) assembly inhibition by PEG-FUD in mCAF & hCAF.** (A) Immunofluorescence staining of FN assembled by mCAF 48 hr after incubation of a vehicle control (Ctrl_PBS) or PEG-FUD (500 nM each). Scale bar = 100 µm. (B) FN (+) area changes measured by fluorescence-positive area per number of cells (nuclei). **P<0.005, n=4 per group. (C) Immunofluorescence staining of FN assembled by hCAF 48 hr after incubation of a vehicle control (Ctrl_PBS) or PEG-FUD (250 nM each). (D) FN (+) area changes measured by fluorescence-positive area per number of cells (nuclei). ****P<0.0001, n=5 per group.

281 treated condition (Fig 1C-D). These results provide evidence that PEG-FUD broadly inhibits *in*
282 *vitro* FN assembly by fibroblasts, including FN assembled by mammary CAFs *in vitro*.
283
284 **FN is highly expressed in 4T1 mammary tumors compared to other organs**
285 FN expression is significantly increased in human breast tumors compared to normal breast tissue
286 and is correlated with poor prognosis(43,44). To investigate the therapeutic potential of PEG-FUD
287 to inhibit FN assembly, we chose the aggressive 4T1 pre-clinical murine model that mimics human
288 TNBC(45). Before testing the therapeutic efficacy of PEG-FUD, we set out to validate and
289 quantify the increase in circulating and peritumoral FN in the 4T1 tumor model. To accomplish
290 this goal, we quantified FN levels in plasma and major organs of normal (non-tumor bearing) and
291 tumor-bearing mice. Plasma FN (pFN) levels were similar in normal mice and in 4T1 tumor-
292 bearing mice (Fig 2A). However, when assessing FN in major organ tissues, we found both soluble
293 FN (sFN) and assembled / insoluble FN (iFN) levels were significantly increased in tumor tissues
294 compared to all other major organs in both normal and tumor-bearing mice (Fig 2B-C).
295 Specifically, 4T1 mammary tumors had more than 20-fold higher FN than normal mammary
296 glands. Analysis of FN in the kidney, heart, liver, and spleen tissue revealed no significant
297 difference in sFN or iFN between tumor-bearing and non-tumor-bearing mice. Notably, the lung
298 tissue of 4T1 tumor-bearing mice had a trend toward increased iFN compared to the lungs of non-
299 tumor-bearing mice. Similarly, others have identified an increased accumulation of total FN in
300 metastatic 4T1 lesions isolated from multiple organ sites of tumor-bearing mice compared to non-
301 tumor-bearing normal organs(46). Overall, our results validate that 4T1 tumors are high in sFN
302 and iFN expression, making it a suitable model to study the anti-cancer effects of inhibiting FN
303 assembly with PEG-FUD.

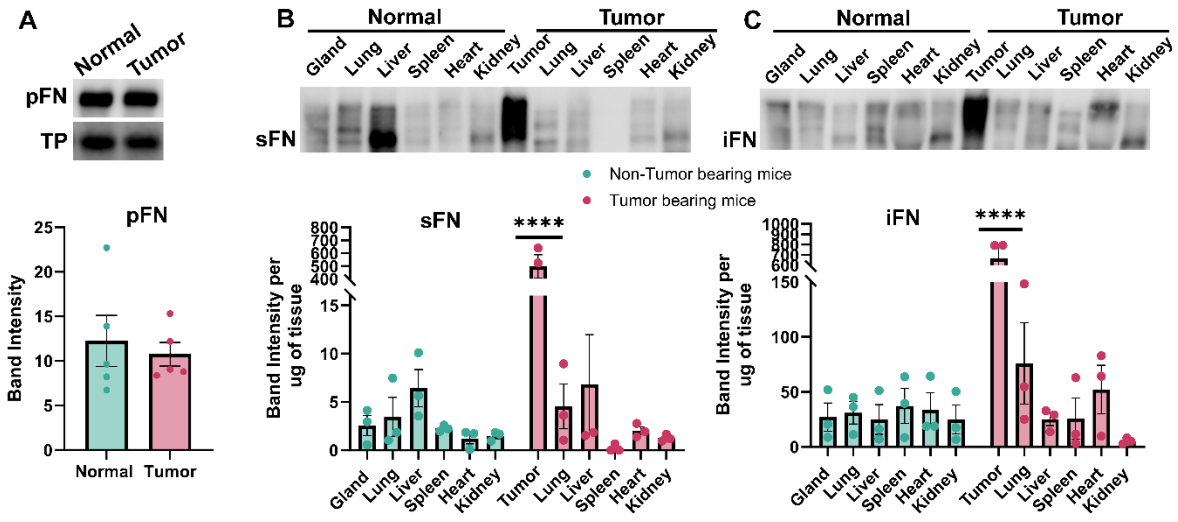

Figure 2: **High FN expression in 4T1 mammary tumors compared to other organs**. 9-week-old female BALB/c mice were injected with 2×10^5 4T1 cells into the fourth mammary fat pad and allowed to grow for 4 weeks. (A) Representative western blot and quantification of plasma FN (pFN) in normal, non-tumor bearing mice and in 4T1 tumor bearing mice. A representative total protein (TP) band is shown as a loading control. n=5 per group (B-C) Representative western blot and quantification of soluble FN (sFN) and insoluble FN (iFN) in multiple tissues of normal and 4T1 tumor bearing mice. The term "gland and tumor" refers to the mammary gland and mammary tumor. ****P<0.0001, n=3 per group

PEG-FUD treatment reduced 4T1 tumor growth and decreased intratumoral FN levels

Previously we have demonstrated that PEG-FUD targets and accumulates in 4T1 mammary tumors compared to other organs using multiple imaging modalities(36). To investigate the therapeutic efficacy of targeting FN in the TME, we treated 4T1 orthotopic mammary tumors with the FN-targeting peptide, PEG-FUD, as an anti-cancer agent. One-week after 4T1 cancer cell injection into the right 4th mammary fat pad, when the average tumor size reached ~50 mm^3, mice were subcutaneously injected with either vehicle control (Ctrl_PBS) or 12.5 mg/kg (in peptide equivalent) of PEG-FUD, PEG-mFUD or PEG-FmFUD every 48hr for a total of 10 doses (Fig 3A). The mFUD and FmFUD control peptides are mutated versions of WT FUD with 7 or 10 mutation sites, respectively (Supplemental Fig 1A). Our results showed that PEG-FUD treatment

315 slowed tumor growth after just 4 doses compared to the control groups. Similarly, at endpoint (10
316 doses) PEG-FUD significantly reduced tumor volume compared to Ctrl_PBS and PEG-FmFUD
317 (Fig 3B-C). The control peptide, PEG-mFUD, had a partial effect in reducing tumor growth, while
318 tumor growth in the PEG-FmFUD treated mice was similar to the vehicle, Ctrl_PBS-treated mice.
319 This was not surprising, as we previously showed that PEG-mFUD partially inhibits b-FUD
320 binding to FN at high concentrations *in vitro*(36), and the partial binding of PEG-mFUD to FN
321 might be explained by the remaining (non-mutated) binding sites for FN present in PEG-mFUD
322 (Supplemental Fig 1A). This is further supported by the result from the fully mutated control
323 peptide, PEG-FmFUD, which has additional mutations in FN binding sites and did not bind to FN
324 in enzyme-linked competitive binding assay, suggesting that the additional mutations reduced
325 binding to FN *in vitro* (Supplemental Fig 2A).
326 As PEG-FUD binds to the 70-kDa region of cellular and plasma FN, we evaluated the
327 pharmacological effect of PEG-FUD on both plasma and intratumoral FN. First, we evaluated
328 circulating FN in the plasma isolated from whole blood using western blot analysis. Results
329 showed no changes in pFN levels between Ctrl_PBS and peptide treatment groups (Fig 3D). To
330 detect FN in tumors, flash frozen tumor tissue was lysed into two separate fractions, DOC-soluble
331 fraction containing sFN and DOC-insoluble fraction containing assembled iFN(47). Again, we
332 quantified FN levels in each tumor lysate fraction by western blot. As expected, 10 doses of PEG-
333 FUD significantly reduced iFN while no changes in sFN were observed (Fig 3E-F). As mentioned
334 previously, the shift in tumor growth rate in response to PEG-FUD occurred early in the treatment
335 time course. Therefore, we evaluated a subset of tumors from the Ctrl_PBS and PEG-FUD groups
336 at an earlier treatment time point (after 6 doses). Total FN levels in these tumors were assessed by
337 immunofluorescence staining. After just 6 doses of PEG-FUD, image analysis demonstrated a

338 significant decrease in the levels of total FN as quantified by mean fluorescent intensity per field

339 of view (Fig 3G-H).

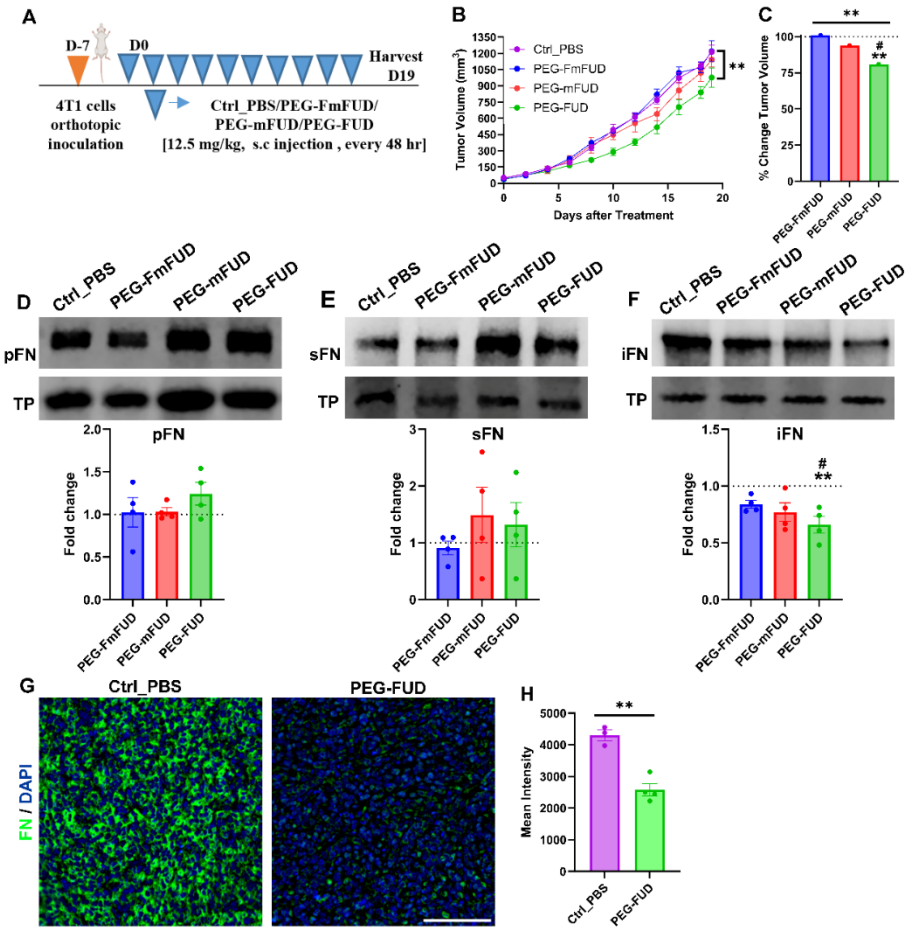

Figure 3: **PEG-FUD significantly reduced 4T1 tumor growth and FN in the TME** (A) Experimental design for therapeutic treatment. 9-week-old, female BALB/c mice were injected with 2×10^5 4T1 cells into the 4th mammary fat pad. Mice were subcutaneously (s.c) treated with vehicle control (Ctrl_PBS), PEG-FmFUD, PEG-mFUD, or PEG-FUD (10 doses of 12.5 mg/kg peptide) when tumors reached ~50 mm^3. (B) 4T1 tumor growth post Ctrl_PBS & peptide treatments. **P<0.005, n=4 per group. (C). % Change in 4T1 tumor volume from Ctrl_PBS to mice treated with PEG-FmFUD, PEG-mFUD, or PEG-FUD. # indicates significant fold change relative to significance from vehicle control (Ctrl_PBS). **P<0.005, n=4 per group. (D-F) Representative western blots and quantification of pFN, sFN, and iFN post Ctrl_PBS and peptide treatments. A representative total protein (TP) band is shown as a loading control. The graphs represent normalized band intensities to Ctrl_PBS treatment. # indicates significance from vehicle control (Ctrl_PBS) **P<0.005, n=4 per group (G-H) Immunofluorescence staining and quantification of FN in 4T1 tumors from Ctrl_PBS and PEG-FUD treated mice (6 doses of 12.5 mg/kg peptide). Scale bar = 100 µm. **P<0.005, n=3-4 per group.

340 FN is known to function as a provisional matrix for the deposition and structural organization of
341 additional fibrotic matrix proteins(24). Thus, the reduction in iFN levels in PEG-FUD treated
342 tumors led us to investigate potential changes in other peritumoral ECM proteins. Furthermore,
343 previous *in vivo* studies using FUD as an anti-fibrotic agent in other fibrotic diseases demonstrated
344 that FUD not only blocked FN assembly, but the treatment was accompanied by a reduction in
345 collagen deposition(31,34). To assess alterations in other ECM proteins in the 4T1 TME post-
346 PEG-FUD treatment, we probed tumor lysates for FN-interacting matrix proteins that we and
347 others have identified in the 4T1 tumor model(48–50). We investigated the levels of collagen
348 (COL1A1), tenascin-C (TNC) and periostin (POSTN) in the DOC-insoluble fraction of tumor
349 lysates by western blot. Surprisingly, our findings showed no significant changes in COL1A1,
350 TNC or POSTN (Supplemental Fig 3A-C). While the protein levels of COL1A1 remained
351 unchanged with PEG-FUD treatment, the possibility remained that collagen fiber architecture may
352 be altered due to the reduction in assembled FN. To evaluate collagen fiber architecture, we stained
353 sections with PSR and conducted second harmonic generation imaging of collagen on thick tumor
354 sections. Interestingly, PEG-FUD treatment did not alter collagen fiber area, nor did we observe
355 any apparent difference in fiber architecture in any of the treatment groups (Supplemental Fig 3D-
356 E). One possibility for this result may be due to the reduced, but not eliminated, level of iFN,
357 which allows for the residual FN fibrils to act as a template for collagen and other ECM deposition
358 in the TME.
359
360 **No significant toxicities were detected in PEG-FUD treated mice**
361 Drug-induced toxicity is a major concern in developing new treatments for breast cancer patients.
362 To validate the safe use of PEG-FUD as a therapeutic agent, we conducted a series of standard

363 toxicity and histologic assessments. No significant body weight changes or signs of distress were
364 observed in mice within Ctrl_PBS or peptide treatment groups (Fig 4A). The spleen weights of
365 control and peptide treated mice were not significantly different (Fig 4B). CBC analysis indicated
366 no changes in white blood cells (WBC), lymphocytes (LYM), monocytes (MON), or neutrophils
367 (NEU) (Fig 4C). Additionally, platelet levels were noted to be higher with PEG-FUD treatment
368 although not statistically significant from control groups (Fig 4D). The platelet count after PEG-
369 FUD treatment remained within the typical range of platelet counts reported in other studies
370 utilizing BALB/c mice(51,52). Histopathologic analysis of kidneys identified mild to moderate
371 intracytoplasmic vacuolation within cortical tubular epithelial cells in all peptide treatment groups.
372 This vacuolar change was not observed in the vehicle treated, Ctrl_PBS group (Supplemental Fig
373 4A). Prior reports show that PEG-linked proteins can induce renal tubular vacuolation at high dose

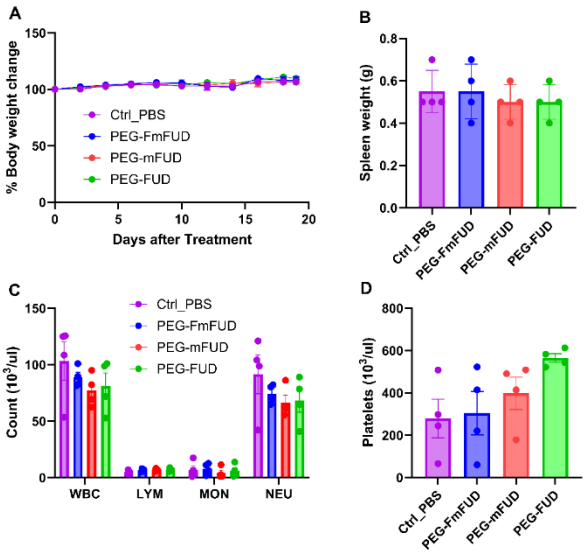

Figure 4: **No changes in toxicity profile post PEG-FUD treatment.** 2×10^5 4T1 tumor cells were injected into the 4th mammary fat pad and allowed to grow to 50 mm^3. Then animals were administered vehicle control (Ctrl_PBS) or 10 peptide treatments via subcutaneous injection every 48 hr. (A) Time course of body weight measurements collected at every treatment period. (B) Quantification of spleen weight measurements at the end of treatment. (C) Complete blood count analysis of white blood cells (WBC), lymphocytes (LYM), monocytes (MON), or neutrophils (NEU) at therapeutic end point. (D) Platelet levels post Ctrl_PBS and peptide treatments. n=4 per group

374 or repetitive low doses, yet modifications were not linked to any changes in clinical pathology or
375 functional indicators(53). Histopathologic analysis of liver showed mild extramedullary
376 hematopoiesis (EMH) in both Ctrl_PBS and peptide treatment groups, with no noted difference in
377 abundance between groups, suggesting the findings may be due to the 4T1 tumor model rather
378 than treatment (Supplemental Fig 4B).
379

380 **PEG-FUD treatment did not affect cell survival or proliferation signaling**

381 FN is known to initiate signaling through integrin adhesion to activate AKT-mediated cell survival
382 pathways and cell proliferation via the MAPK/ERK pathway. Changes in one or both of these
383 pathways could play a role in the observed reduction in tumor size in PEG-FUD-treated mice. To
384 examine the effect of blocking FN assembly by PEG-FUD, we quantified cell survival signaling
385 by assessing total and phosphorylated AKT (p-AKT) levels in tumor lysates. Surprisingly, no
386 changes were observed in total AKT or activated p-AKT (Fig 5A). Next, we assessed ERK-
387 regulated cell proliferation by quantifying total and phosphorylated ERK (p-ERK). Similar to our
388 results with AKT activity, we found no changes in ERK activation in response to PEG-FUD
389 treatment (Fig 5B). Additionally, we examined two well-known cell proliferation markers, PCNA
390 in tumor lysates after 10 doses of peptide treatment and the area of Ki67+ cells after 6 dose of
391 peptide treatment, using western blotting and immunofluorescence, respectively. Consistent with
392 the above findings, we did not detect a change in either marker of cell proliferation in response to
393 PEG-FUD treatment compared to control groups (Fig 5C-E). Although these findings contradict
394 previous research showing that inhibiting FN decreased proliferation(28,30,31), this may be
395 explained by a difference in orthotopic tumor models or differences in growth factors present in
396 the TME of 4T1 tumors that could maintain proliferation signaling.

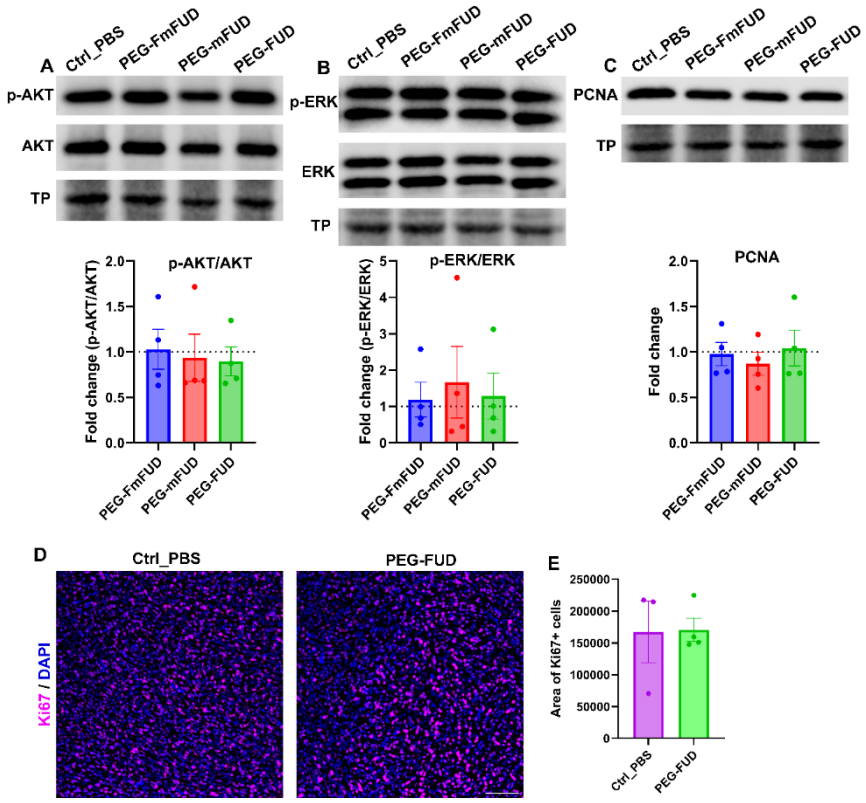

Figure 5: **No changes in cell survival / proliferation signaling post PEG-FUD treatment.** (A-C) Representative western blots and quantification of proliferation markers AKT, ERK and PCNA post vehicle control (Ctrl_PBS) and peptide treatments (10 doses of 12.5 mg/kg peptide). A representative total protein (TP) band is shown as a loading control. The graphs represent normalized band intensities to Ctrl_PBS treatment. (D) Representative immunofluorescent images stained for proliferation marker Ki67 post Ctrl_PBS and PEG-FUD treatment (6 doses of 12.5 mg/kg peptide). (E) Quantification of Ki67+ area from D.

Treatment with PEG-FUD reduced α5 integrin and FAK protein expression and promoted caspase-3 mediated cell death

Next, we sought to interrogate FN-mediated focal adhesions and downstream apoptotic signaling as part of the mechanism by which PEG-FUD therapy inhibits tumor growth. Integrin α5β1 is the primary receptor for FN that binds sFN and initiates the assembly of FN into a fibrillar matrix(54). In addition, the binding of integrins to FN activates intracellular signaling pathways downstream of focal adhesions(55). To determine whether adhesion-mediated signaling is disrupted in response

405 to PEG-FUD, we quantified the level of α5 and β1 integrins by western blot analysis. PEG-FUD
406 treatment resulted in a significant reduction in the tumor levels of integrin α5 (Fig 6A). In contrast,
407 PEG-FUD therapy did not affect β1 integrin (Fig 6B). β1 integrins form complexes with multiple
408 alpha integrins subunits to bind several ECM proteins found in the TME(56). Thus, the lack of β1
409 integrin specificity for FN is one possible rationale for the modulation of α5, but not β1 integrin,
410 in response to PEG-FUD treatment. Due to the reduction in iFN and α5 integrin levels, we next
411 evaluated the effect of PEG-FUD on the focal adhesion signaling through focal adhesion kinase
412 (FAK). FAK is a master regulator of cell adhesion signaling upon integrin activation and
413 clustering(57). Strikingly, we observed a significant reduction in total FAK protein levels in PEG-
414 FUD treated tumors compared to controls (Fig 6C). Taken together, these findings indicate that
415 inhibiting FN assembly with PEG-FUD alters FAK-dependent integrin-mediated cell adhesion.
416 In the literature, FN knockdown, blockade of FN receptor integrin α5β1, and alterations in FAK
417 have been shown to induce anoikis, a type of programmed cell death that results from a loss of
418 cell-ECM attachment(58,59). To investigate the effect of FN inhibition by PEG-FUD in mediating
419 cell death, we probed for cell death markers at both early and late treatment time points (6 or 10
420 doses of PEG-FUD). We confirmed the induction of cell death by PEG-FUD by a statistically
421 significant increase in cleaved caspase-3 levels from whole tumor lysates collected from mice that
422 received 10 doses of PEG-FUD compared to control-treated tumor groups (Fig 6D). Tumors
423 harvested from mice that received 6 doses of PEG-FUD showed a qualitative increase in the
424 presence of tumor necrosis identified in H&E stained sections (Fig 6E). Additionally,
425 representative serial sections from each treatment group were assessed by TUNEL assay. We
426 identified large TUNEL positive regions at the core of PEG-FUD treated tumors that are not

427 observed in the vehicle control (Ctrl_PBS) treated tumors (Fig 6F). Altogether, these results

428 suggest that PEG-FUD induced cell death by inhibiting FN-integrin-mediated cell adhesion.

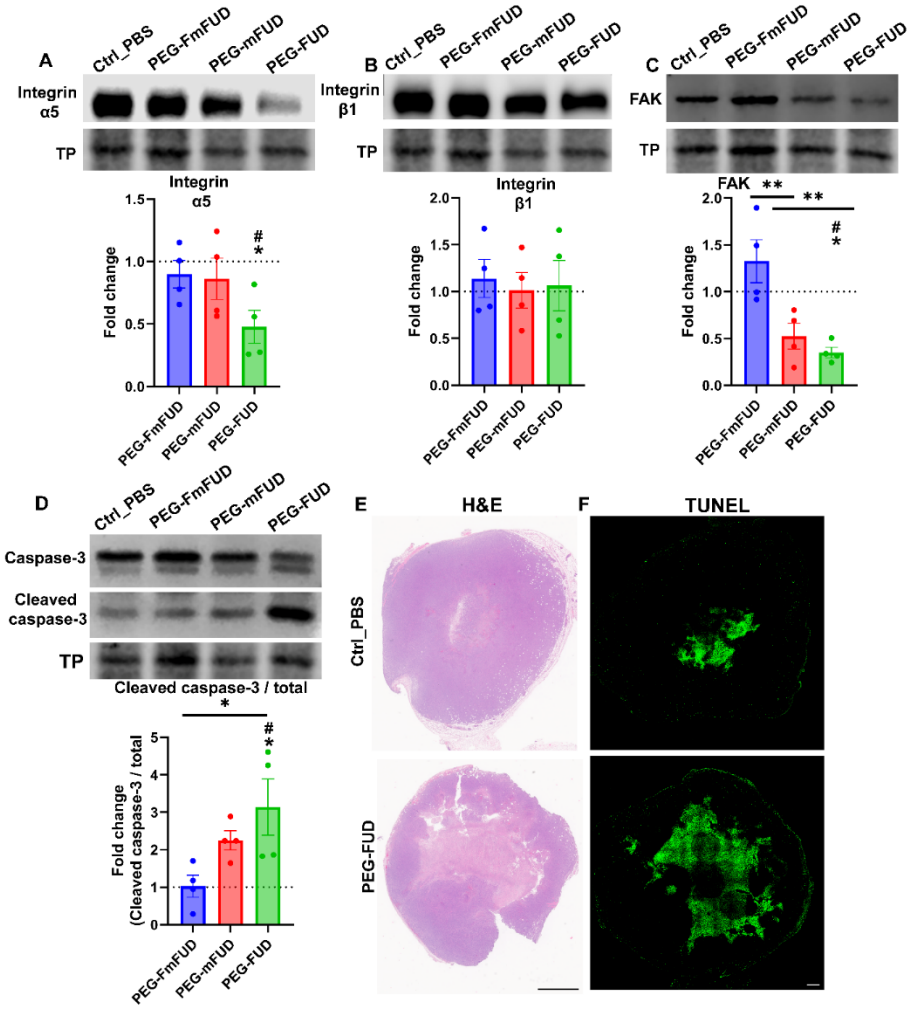

Figure 6: **PEG-FUD alters integrin mediated adhesion signaling and cell death.** (A-D) Representative western blots and quantification of Integrin α5, Integrin β1, FAK, caspase-3 and cleaved caspase-3 from 4T1 tumor lysates treated with vehicle control (Ctrl_PBS) and peptides (10 doses of 12.5 mg/kg peptide). A representative total protein (TP) band is shown as a loading control. The graphs represent normalized band intensities to Ctrl_PBS treatment. # indicates significant fold change relative to significance from vehicle control (Ctrl_PBS). *P<0.05, **P<0.005, n=4 per group (E) Representative images of H&E staining and TUNEL staining of 4T1 tumor sections from mice treated with Ctrl_PBS and PEG-FUD (6 doses of 12.5 mg/kg peptide). H&E Scale bar = 100 µm; TUNEL Scale bar = 500 µm.

429

430 **PEG-FUD primes the mammary TME for enhanced anti-tumor efficacy of doxorubicin**

431 The identification of PEG-FUD-mediated tumor cell death led us to hypothesize that PEG-FUD
432 not only has intrinsic anti-cancer potential but may also synergistically improve the tumor response
433 to chemotherapy. Others have demonstrated that the overexpression of FAK, which is identified in
434 multiple tumors, plays a critical role in suppressing tumor cell death and facilitating resistance to
435 Dox(60,61). Based on these findings and our evidence for PEG-FUD to robustly inhibit FAK
436 protein levels in the 4T1 TME, we tested the ability of PEG-FUD pre-treatment to improve the
437 response of a commonly used chemotherapeutic drug, Dox, in the 4T1 tumor model. 4T1
438 orthotropic tumors were established similarly to the PEG-FUD monotherapy approach with
439 treatment starting when the average tumor size reached ~50 mm^3. Mice were randomized into
440 treatment groups and subcutaneously injected with either vehicle control (Ctrl_PBS) or 12.5 mg/kg
441 (in peptide equivalent) of PEG-FUD or PEG-FmFUD every 48 hr for 4 doses. At the 4-dose
442 timepoint (when a shift in tumor growth was noted, Fig 3B), we initiated intraperitoneal
443 administration of Dox at 5mg/kg every 72 hr with continued peptide treatment (experimental
444 design outlined in Fig 7A). Combinatorial treatment of PEG-FUD and Dox resulted in a significant
445 reduction in tumor growth by ~60% to vehicle control and by an additional ~30% to Dox alone,
446 demonstrating that PEG-FUD co-treatment increased the efficacy of Dox therapy in the 4T1 TNBC
447 model (Fig 7B-C). Mice treated with Dox exhibited loss of body and spleen weight due to the well-
448 known systemic toxicity of Dox, but no additive effect was detected with co-treatment with PEG-
449 FUD (Fig 7D-E). These findings provide evidence that reducing FN with PEG-FUD improves
450 chemotherapeutic response.
451
452

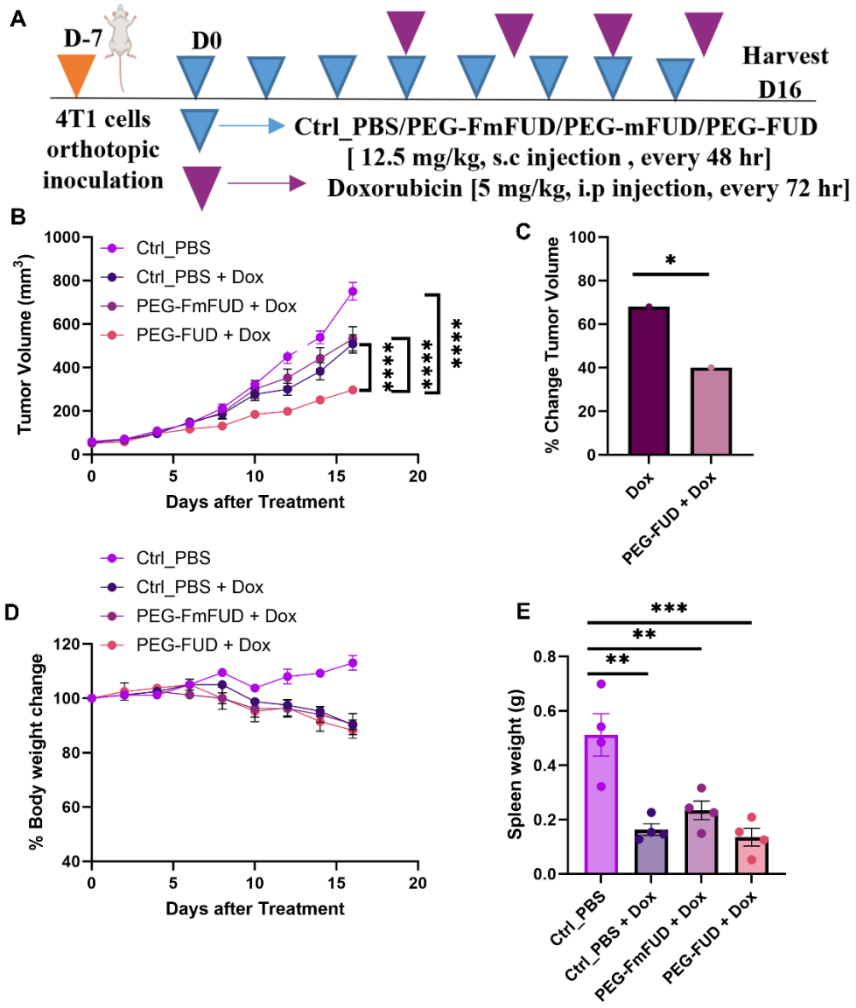

Figure 7: **PEG-FUD combined with Doxorubicin resulted in enhanced efficacy without additional toxicity.** (A) Experimental design for therapeutic treatment. 9-week-old, female BALB/c mice were injected with 2×10^5 4T1 cells into the 4th mammary fat pad. Mice were subcutaneously (s.c) treated with 4 doses of vehicle control (Ctrl_PBS), PEG-FmFUD, or PEG-FUD at 12.5 mg/kg every 48 hrs once tumors reached ~ 50 mm^3. Upon the 4th dose of PEG-FUD, Doxorubicin (Dox) was administered intraperitoneally (i.p) at 5mg/kg every 72 hr with continued peptide treatment until day 16 post 4T1 tumor cell inoculation. (B) 4T1 tumor growth post Ctrl_PBS and combined treatments. ****P<0.0001, n=4 per group. (C). % Change in 4T1 tumor volume from Ctrl_PBS to mice treated with Dox and PEG-FUD + Dox. *P<0.05, n=4 per group. (D) Time course of body weight measurements collected at every treatment period post vehicle control (Ctrl_PBS), Dox and peptide + Dox combination treatments. (E) Quantification of spleen weights post Ctrl_PBS, Dox and peptide combination treatments at the end of treatment period. **P<0.005, ***P<0.001, n=4 mice per group.

455 **Discussion**

456 In this study, we investigated the anti-cancer effects of targeting FN matrix assembly in the TME
457 using PEG-FUD. Several FN-targeting strategies have been developed and demonstrated promise
458 in the diagnosis, therapy, and image-guided interventions of a variety of malignancies(62). For
459 example, antibodies that detect the EDA domain of cellular FN have shown promise for solid
460 tumor diagnostics(63). Additional studies expanded on the utility of targeting FN by developing
461 antibody-drug conjugates using an EDA-antibody with anti-IL-2(64), EDA expressing CAR-T
462 cells(65), or developing fibrin-FN binding peptides conjugated with Dox(66) for enhanced
463 therapeutic efficacy and reduced systemic toxicities. Some of these approaches made it to early-
464 phase human trials, however, they have yet to be FDA-approved for the clinical treatment of breast
465 cancer. Thus, developing new therapeutic approaches to target FN in the TME is both timely and
466 promising.

467 Here, we take advantage of targeting FN with PEG-FUD. PEG-FUD binds with high affinity to
468 the 70-kDa N-terminus and inhibits the assembly of all sources of FN (cellular and plasma derived
469 FN). This is essential since both sources of FN can be deposited in the tumor matrix(67,68). We
470 previously reported that PEG-FUD accumulates and is maintained in 4T1 tumors for prolonged
471 periods compared to FUD alone(36). Our current *in vitro* data demonstrate that PEG-FUD
472 successfully inhibited the assembly of endogenous FN assembled by mammary CAFs (Fig 1). In
473 addition, we demonstrated that PEG-FUD is effective when given in therapeutic doses to reduce
474 the assembly of tumor FN (decreased iFN levels) and to suppress 4T1 tumor growth (Fig 3).
475 Therefore, like prior studies we confirmed that the PEGylation of the FUD peptide retained the
476 ability to block FN assembly(33,34,36). Together these data demonstrate the utility of PEG-FUD
477 not only for tumor diagnostics but also as an anti-breast cancer therapeutic.

478 Mechanistically we determined that PEG-FUD treatment significantly reduced levels of α5
479 integrin, a major adhesion receptor for FN. Integrin binding to FN mediates intracellular signaling
480 to regulate cellular processes such as cell growth, proliferation, and migration(69–71). Despite the
481 significant reduction in α5 integrin and FAK, we did not observe differences in proliferation or
482 survival signaling through ERK or AKT, respectively. This result contradicts previous observations
483 that FUD/puR4 peptide decreased ERK phosphorylation without affecting FAK or AKT
484 phosphorylation(31). However, the difference between our findings and those of Ghura et al. may
485 be explained by differences in model systems (immune competent vs immune compromised),
486 treatment conditions (PEG-FUD vs FUD), and identification of altered signaling pathways (within
487 tumors vs in cell culture). Furthermore, ERK and AKT activation can occur independent of FN-
488 FAK mediated signaling. In support of this hypothesis, a study utilizing an integrin antagonist 1a-
489 RGD in glioblastoma cells showed that by inhibiting cell adhesion, FAK activation decreased
490 without altering ERK and AKT-dependent pathways(72). It is also plausible that the reduction in
491 iFN could release growth hormones normally sequestered in the matrix that become available to
492 bind and activate pathways downstream of growth factor receptors(73–76).

493 In our study, the loss of α5 and FAK in the TME in response to PEG-FUD is notable. While we do
494 not know the temporal sequence of α5 integrin vs FAK down-regulation, the functional inhibition
495 of α5β1 integrin activation has been shown to reduce total FAK expression and protein levels(77).
496 Others have also demonstrated that caspase-mediated FAK cleavage (degradation of FAK) causes
497 focal adhesion complexes to disassemble(78), suggesting the activation of caspase signaling could
498 reduce levels of FAK and α5 integrin. Importantly, the disassembly of focal adhesions down stream
499 of caspase activation interferes with integrin-mediated survival signaling, thereby propagating the
500 cell death program(78). In line with these studies, we identified an increase in TUNEL-positive

501 staining and caspase-3 mediated cell death in PEG-FUD-treated tumors. Multiple studies have
502 shown that integrin adhesion to FN can induce anoikis resistance and reduce apoptosis(58,79).
503 Moreover, FAK itself has been identified to play a critical role in suppressing cell death(80–83).
504 FAK has been shown to directly bind to the death domain of receptor-interacting protein (RIP) to
505 suppress apoptosis(61). RIP provides proapoptotic signals that are suppressed upon binding to
506 FAK, thus blocking the FAK-RIP interaction or reducing total FAK levels shifts cells toward
507 caspase-mediated cell death. Taken together, our findings suggest that PEG-FUD effectively
508 blocked FN assembly within the TME resulting in decreased α5 integrin and FAK levels, leading
509 to apoptosis via the activation of caspase-3 cleavage. This results in an overall reduction in tumor
510 growth, demonstrating PEG-FUD as an effective single agent therapy to target pre-clinical breast
511 cancer.

512 Our characterization of the tumor response to PEG-FUD also demonstrates the promise of
513 targeting FN to improve standard-of-care cancer therapies. For many solid tumors, including
514 TNBC, the first-line treatment is chemotherapy. However, the ECM of solid breast tumors
515 activates mechanisms of drug resistance that significantly impede clinical therapies(84–86). Other
516 pre-clinical mammary tumor studies have shown that Pirfenidone, an FDA approved antifibrotic
517 drug for idiopathic pulmonary fibrosis, normalizes the tumor ECM for enhanced chemotherapy
518 response, demonstrating the value of ECM normalization(87). This study focused on the action of
519 pirfenidone to block TGF-b signaling and downstream ECM deposition, which led to increased
520 drug penetration. Our data suggest that the anti-fibrotic impact of PEG-FUD not only reduces iFN
521 within tumors but also alleviates ECM-mediated mechanisms of drug resistance through the
522 reduction of FAK. In line with our findings, van Nimwegen et al. illuminated a mechanism by
523 which adhesion-mediated stress fiber formation and FAK activation suppressed Dox-induced

524 apoptosis(60). Based on these results, we hypothesized that by reducing tumoral FN and inhibiting
525 α5 integrin and FAK, PEG-FUD sufficiently primed the TME for improved chemotherapy
526 response. Indeed, when 4T1 tumors were primed with PEG-FUD followed by combined treatment
527 with Dox + PEG-FUD we quantified a 60% decrease in tumor growth compared to vehicle control
528 and 30% compared to Dox monotherapy. Notably, combinatorial treatment of PEG-FUD and Dox
529 did not increase the systemic toxicity of Dox (Fig 7). Thus, PEG-FUD therapy is an effective
530 strategy to improve the efficacy of standard-of-care chemotherapy in 4T1 TNBC model.
531

532 **Conclusion**

533 In summary, we have demonstrated the efficacy of PEG-FUD to target FN in 4T1 triple-negative
534 tumors and improve response to standard chemotherapy. We have characterized changes in the
535 TME in response to PEG-FUD treatment and identified a mechanism where the reduction in iFN
536 leads to a significant decrease in α5 integrin and FAK levels. Further, these changes in cell
537 adhesion increased tumor cell death and blocked tumor growth. Strikingly, the tumor response to
538 PEG-FUD therapy was sufficient to prime the TME into a non-tumor-supporting
539 microenvironment and significantly enhance the efficacy of Dox therapy. As we previously
540 demonstrated PEG-FUD can also target the metastatic microenvironment(36), our future studies
541 will explore PEG-FUD as an effective treatment for metastatic breast cancer.
542

543 Acknowledgments: This work was supported by the National Cancer Institute funding to SMP
544 (R01CA206458, and R01CA179556) and R21CA252579 to SMP and GSK. Additionally, this
545 research was supported by the University of Wisconsin-Carbone Cancer Center, More for Stage
546 IV Research Award to SMP.

547 Author contributions: MKG conceptualized the study, conducted experiments, analyzed and
548 interpreted data, organized figures, wrote and edited the manuscript. HJL conducted experiments,
549 analyzed data, and edited the manuscript. DRI assisted with all animal experiments. NG prepared
550 PEGylated FUD, conducted experiments, analyzed and edited the manuscript. BB assisted with
551 data analysis, interpretation and edited the manuscript. MH conducted the histopathologic
552 assessment and edited the manuscript. GSK acquired funding, conceptualized the study,
553 interpreted data, and edited the manuscript. SMP acquired funding, conceptualized the study,
554 oversaw the experiments and data collection, interpreted analysis, wrote and edited the manuscript.

555

556 **References**

557 1. Conklin MW, Keely PJ. Why the stroma matters in breast cancer: Insights into breast
558 cancer patient outcomes through the examination of stromal biomarkers. Cell Adh
559 Migr [Internet]. 2012 [cited 2024 Jul 14];6(3):249–60. Available from:
560 https://www.tandfonline.com/action/journalInformation?journalCode=kcam20

561 2. Oskarsson T. Extracellular matrix components in breast cancer progression and
562 metastasis. Breast [Internet]. 2013 Aug 1 [cited 2024 Jul 14];22 Suppl 2(S2). Available
563 from: https://pubmed.ncbi.nlm.nih.gov/24074795/

564 3. Fertal SA, Poterala JE, Ponik SM, Wisinski KB. Stromal Characteristics and Impact on
565 New Therapies for Metastatic Triple-Negative Breast Cancer. Cancers (Basel)
566 [Internet]. 2022 Mar 1 [cited 2024 Jul 14];14(5). Available from:
567 https://pubmed.ncbi.nlm.nih.gov/35267548/

568 4. Anttila MA, Tammi RH, Tammi MI, Syrjänen KJ, Saarikoski S V, Kosma VM. High Levels
569 of Stromal Hyaluronan Predict Poor Disease Outcome in Epithelial Ovarian Cancer 1.
570 Cancer Res [Internet]. 2000 [cited 2024 Jun 30];60:150–5. Available from:
571 http://aacrjournals.org/cancerres/article-pdf/60/1/150/3241293/ch010000150p.pdf

572 5. Parker AL, Bowman E, Zingone A, Ryan BM, Cooper WA, Kohonen-Corish M, et al.
573 Extracellular matrix profiles determine risk and prognosis of the squamous cell
574 carcinoma subtype of non-small cell lung carcinoma. Genome Medicine 2022 14:1

575 [Internet]. 2022 Nov 21 [cited 2024 Jun 30];14(1):1–29. Available from:
576 https://genomemedicine.biomedcentral.com/articles/10.1186/s13073-022-01127-6

577 6. Yuzhalin AE, Urbonas T, Silva MA, Muschel RJ, Gordon-Weeks AN. A core matrisome
578 gene signature predicts cancer outcome. Nature Publishing Group [Internet]. 2018
579 [cited 2024 Jun 30];118. Available from: http://matrisomeproject.mit.edu/

580 7. Bae YK, Kim A, Kim MK, Choi JE, Kang SH, Lee SJ. Fibronectin expression in
581 carcinoma cells correlates with tumor aggressiveness and poor clinical outcome in
582 patients with invasive breast cancer. Hum Pathol. 2013 Oct 1;44(10):2028–37.

583 8. Conklin MW, Eickhoff JC, Riching KM, Pehlke CA, Eliceiri KW, Provenzano PP, et al.
584 Aligned Collagen Is a Prognostic Signature for Survival in Human Breast Carcinoma.
585 Am J Pathol [Internet]. 2011 [cited 2022 Mar 5];178(3):1221. Available from:
586 /pmc/articles/PMC3070581/

587 9. Esbona K, Yi Y, Saha S, Yu M, Van Doorn RR, Conklin MW, et al. The Presence of
588 Cyclooxygenase 2, Tumor-Associated Macrophages, and Collagen Alignment as
589 Prognostic Markers for Invasive Breast Carcinoma Patients. American Journal of
590 Pathology [Internet]. 2018 Mar 1 [cited 2024 Jun 29];188(3):559–73. Available from:
591 http://ajp.amjpathol.org/article/S0002944017302833/fulltext

592 10. Liu J, Liao S, Diop-Frimpong B, Chen W, Goel S, Naxerova K, et al. TGF-β blockade
593 improves the distribution and efficacy of therapeutics in breast carcinoma by
594 normalizing the tumor stroma. Proc Natl Acad Sci U S A [Internet]. 2012 Oct 9 [cited
595 2024 Jun 16];109(41):16618–23. Available from:
596 www.pnas.org/cgi/doi/10.1073/pnas.1117610109

597 11. Vandenbroucke RE, Libert C. Is there new hope for therapeutic matrix
598 metalloproteinase inhibition? Nature Publishing Group [Internet]. 2014 [cited 2024
599 Jun 16]; Available from: www.nature.com/reviews/drugdisc

600 12. Mariathasan S, Turley SJ, Nickles D, Castiglioni A, yuen K, Wang yulei, et al. TGFβ
601 attenuates tumour response to PD-L1 blockade by contributing to exclusion of T
602 cells. 2018;

603 13. Coulson R, Liew SH, Connelly AA, Yee NS, Deb S, Kumar B, et al. The angiotensin
604 receptor blocker, Losartan, inhibits mammary tumor development and progression
605 to invasive carcinoma. Oncotarget [Internet]. 2017 [cited 2024 Jun 16];8(12):18640–
606 56. Available from: www.impactjournals.com/oncotarget/

607 14. Sparano JA, Bernardo P, Stephenson P, Gradishar WJ, Ingle JN, Zucker S, et al.
608 Randomized Phase III Trial of Marimastat Versus Placebo in Patients With Metastatic

Breast Cancer Who Have Responding or Stable Disease After First-Line Chemotherapy: Eastern Cooperative Oncology Group Trial E2196. J Clin Oncol [Internet]. 2004 [cited 2024 Jun 16];22:4683–90. Available from: www.jco.org

15. Keiser HR, Sjoerdsma A. Studies on beta-aminopropionitrile in patients with scleroderma. Clinical Pharmacology andTherapeutics. 1967;8(4):593–602.

16. Giaccone G, Bazhenova LA, Nemunaitis J, Tan M, Juhász E, Ramlau R, et al. A phase III study of belagenpumatucel-L, an allogeneic tumour cell vaccine, as maintenance therapy for non-small cell lung cancer. Eur J Cancer [Internet]. 2015 Nov 1 [cited 2024 Jun 16];51(16):2321–9. Available from: http://www.ejcancer.com/article/S0959804915007418/fulltext

17. Sleeboom JJF, van Tienderen GS, Schenke-Layland K, van der Laan LJW, Khalil AA, Verstegen MMA. The extracellular matrix as hallmark of cancer and metastasis: From biomechanics to therapeutic targets. Sci Transl Med [Internet]. 2024 Jan 3 [cited 2024 Nov 3];16(728). Available from: https://www.science.org/doi/10.1126/scitranslmed.adg3840

18. Tomko LA, Hill RC, Barrett A, Szulczewski JM, Conklin MW, Eliceiri KW, et al. Targeted matrisome analysis identifies thrombospondin-2 and tenascin-C in aligned collagen stroma from invasive breast carcinoma. Scientific Reports 2018 8:1 [Internet]. 2018 Aug 28 [cited 2022 Mar 5];8(1):1–11. Available from: https://www.nature.com/articles/s41598-018-31126-w

19. Spada S, Tocci A, Di Modugno F, Nisticò P. Fibronectin as a multiregulatory molecule crucial in tumor matrisome: from structural and functional features to clinical practice in oncology. Journal of Experimental & Clinical Cancer Research 2021 40:1 [Internet]. 2021 Mar 17 [cited 2024 Jul 14];40(1):1–14. Available from: https://jeccr.biomedcentral.com/articles/10.1186/s13046-021-01908-8

20. Hebert JD, Myers SA, Naba A, Abbruzzese G, Lamar JM, Carr SA, et al. Proteomic profiling of the ECM of xenograft breast cancer metastases in different organs reveals distinct metastatic niches. Cancer Res [Internet]. 2020 Apr 1 [cited 2024 Nov 3];80(7):1475–85. Available from: /cancerres/article/80/7/1475/647712/Proteomic-Profiling-of-the-ECM-of-Xenograft-Breast

21. Hynes RO, Yamada KM. Fibronectins: Multifunctional Modular Glycoproteins. [cited 2024 May 13]; Available from: http://rupress.org/jcb/article-pdf/95/2/369/1641134/369.pdf

642 22. Wierzbicka-Patynowski I, Schwarzbauer JE. The ins and outs of fibronectin matrix
643 assembly. J Cell Sci [Internet]. 2003 Aug 15 [cited 2024 May 13];116(16):3269–76.
644 Available from: https://dx.doi.org/10.1242/jcs.00670

645 23. Mckeown-Longo PJ, Mosher DF. Interaction of the 70,000-mol-wt Amino-terminal
646 Fragment of Fibronectin with the Matrix-assembly Receptor of Fibroblasts. [cited
647 2024 May 2]; Available from: http://rupress.org/jcb/article-
648 pdf/100/2/364/1457627/364.pdf

649 24. Sottile J, Hocking DC. Fibronectin Polymerization Regulates the Composition and
650 Stability of Extracellular Matrix Fibrils and Cell-Matrix Adhesions. Mol Biol Cell.
651 2002;13:3546–59.

652 25. Pankov R, Yamada KM. Fibronectin at a glance. J Cell Sci [Internet]. 2002 Oct 15
653 [cited 2024 Jul 14];115(20):3861–3. Available from:
654 https://dx.doi.org/10.1242/jcs.00059

655 26. Wang K, Wu F, Seo BR, Fischbach C, Chen W, Hsu L, et al. Breast cancer cells alter
656 the dynamics of stromal fibronectin-collagen interactions. Matrix Biol [Internet].
657 2017 Jul 1 [cited 2024 Jul 15];60–61:86. Available from: /pmc/articles/PMC5293676/

658 27. Tomasini-Johansson BR, Kaufman NR, Ensenberger MG, Ozeri V, Hanski E, Mosher
659 DF. A 49-Residue Peptide from Adhesin F1 of Streptococcus pyogenes Inhibits
660 Fibronectin Matrix Assembly *. Journal of Biological Chemistry [Internet]. 2001 Jun 29
661 [cited 2022 Mar 19];276(26):23430–9. Available from:
662 http://www.jbc.org/article/S0021925820783316/fulltext

663 28. Chiang HY, Korshunov VA, Serour A, Shi F, Sottile J. Fibronectin is an important
664 regulator of flow-induced vascular remodeling. Arterioscler Thromb Vasc Biol
665 [Internet]. 2009 Jul 1 [cited 2022 Mar 19];29(7):1074. Available from:
666 /pmc/articles/PMC3091823/

667 29. Altrock E, Sens C, Wuerfel C, Vasel M, Kawelke N, Dooley S, et al. Inhibition of
668 fibronectin deposition improves experimental liver fibrosis. J Hepatol [Internet]. 2015
669 Mar 1 [cited 2022 Mar 19];62(3):625–33. Available from: http://www.journal-of-
670 hepatology.eu/article/S016882781400405X/fulltext

671 30. Valiente-Alandi I, Potter SJ, Salvador AM, Schafer AE, Schips T, Carrillo-Salinas F, et
672 al. Inhibiting fibronectin attenuates fibrosis and improves cardiac function in a model
673 of heart failure. Circulation [Internet]. 2018 [cited 2022 Mar 19];138(12):1236.
674 Available from: /pmc/articles/PMC6186194/

675 31. Ghura H, Keimer M, von Au A, Hackl N, Klemis V, Nakchbandi IA. Inhibition of
676 fibronectin accumulation suppresses TUMOR growth. Neoplasia (United States).
677 2021 Sep 1;23(9):837–50.

678 32. Lee HJ, Tomasini-Johansson BR, Gupta N, Kwon GS. Fibronectin-targeted FUD and
679 PEGylated FUD peptides for fibrotic diseases. Journal of Controlled Release. 2023
680 Aug 1;360:69–81.

681 33. Zbyszynski P, Tomasini-Johansson BR, Peters DM, Kwon GS. Characterization of the
682 PEGylated Functional Upstream Domain Peptide (PEG-FUD): a Potent Fibronectin
683 Assembly Inhibitor with Potential as an Anti-Fibrotic Therapeutic. Pharm Res
684 [Internet]. 2018 Jul 1 [cited 2022 Feb 5];35(7):126. Available from:
685 /pmc/articles/PMC6186450/

686 34. Tomasini-Johansson BR, Zbyszynski PW, Toraason I, Peters DM, Kwon GS. PEGylated
687 pUR4/FUD peptide inhibitor of fibronectin fibrillogenesis decreases fibrosis in
688 murine Unilateral Ureteral Obstruction model of kidney disease. PLoS One [Internet].
689 2018 Oct 1 [cited 2022 May 7];13(10):e0205360. Available from:
690 https://journals.plos.org/plosone/article?id=10.1371/journal.pone.0205360

691 35. Zbyszynski P, Toraason I, Repp L, Kwon GS. Probing the subcutaneous absorption of a
692 PEGylated FUD peptide nanomedicine via in vivo fluorescence imaging. Nano
693 Converg [Internet]. 2019 Dec 1 [cited 2022 Feb 9];6(1):1–15. Available from:
694 https://nanoconvergencejournal.springeropen.com/articles/10.1186/s40580-019-
695 0192-3

696 36. Lee HJ, Gari MK, Inman DR, Rosenkrans ZT, Burkel BM, Olson AP, et al. Multimodal
697 imaging demonstrates enhanced tumor exposure of PEGylated FUD peptide in
698 breast cancer. Journal of Controlled Release. 2022 Oct 1;350:284–97.

699 37. Maurer LM, Tomasini-Johansson BR, Ma W, Annis DS, Eickstaedt NL, Ensenberger
700 MG, et al. Extended binding site on fibronectin for the functional upstream domain of
701 protein F1 of Streptococcus pyogenes. J Biol Chem [Internet]. 2010 Dec 24 [cited
702 2024 Jul 9];285(52):41087–99. Available from:
703 https://pubmed.ncbi.nlm.nih.gov/20947497/

704 38. Ma W, Ma H, Mosher DF. On-Off Kinetics of Engagement of FNI Modules of Soluble
705 Fibronectin by β-Strand Addition. PLoS One [Internet]. 2015 Apr 28 [cited 2024 Jul
706 9];10(4). Available from: https://pubmed.ncbi.nlm.nih.gov/25919138/

707 39. Ishihara S, Inman DR, Li WJ, Ponik SM, Keely PJ. Tumor and Stem Cell Biology
708 Mechano-Signal Transduction in Mesenchymal Stem Cells Induces Prosaposin

Secretion to Drive the Proliferation of Breast Cancer Cells. [cited 2024 May 5]; Available from: http://cancerres.aacrjournals.org/

40. Tomayko MM, Reynolds CP. ancer hemotherapy and harmacology Determination of subcutaneous tumor size in athymic (nude) mice*. Cancer Chemother Pharmacol. 1989;24:148–54.

41. Attieh Y, Clark AG, Grass C, Richon S, Pocard M, Mariani P, et al. Cancer-associated fibroblasts lead tumor invasion through integrin-β3-dependent fibronectin assembly. J Cell Biol [Internet]. 2017 Nov 1 [cited 2024 Jun 17];216(11):3509–20. Available from: https://pubmed.ncbi.nlm.nih.gov/28931556/

42. Tomasini-Johansson BR, Zbyszynski PW, Toraason I, Peters DM, Kwon GS. PEGylated pUR4/FUD peptide inhibitor of fibronectin fibrillogenesis decreases fibrosis in murine Unilateral Ureteral Obstruction model of kidney disease. PLoS One [Internet]. 2018 Oct 1 [cited 2022 Mar 19];13(10):e0205360. Available from: https://journals.plos.org/plosone/article?id=10.1371/journal.pone.0205360

43. Bae YK, Kim A, Kim MK, Choi JE, Kang SH, Lee SJ. Fibronectin expression in carcinoma cells correlates with tumor aggressiveness and poor clinical outcome in patients with invasive breast cancer. Hum Pathol. 2013 Oct 1;44(10):2028–37.

44. Zhang XX, Luo JH, Wu LQ. FN1 overexpression is correlated with unfavorable prognosis and immune infiltrates in breast cancer. Front Genet [Internet]. 2022 Aug 12 [cited 2024 May 13];13. Available from: /pmc/articles/PMC9417469/

45. Pulaski BA, Ostrand-Rosenberg S. Mouse 4T1 Breast Tumor Model. Curr Protoc Immunol [Internet]. 2000 Oct 1 [cited 2024 May 6];39(1):20.2.1-20.2.16. Available from: https://onlinelibrary.wiley.com/doi/full/10.1002/0471142735.im2002s39

46. Zhou Z, Qutaish M, Han Z, Schur RM, Liu Y, Wilson DL, et al. MRI detection of breast cancer micrometastases with a fibronectin-targeting contrast agent. Nat Commun [Internet]. 2015 Aug 12 [cited 2022 Mar 19];6. Available from: /pmc/articles/PMC4557274/

47. McKeown Longo PJ, Mosher DF. Binding of plasma fibronectin to cell layers of human skin fibroblasts. J Cell Biol [Internet]. 1983 Aug 8 [cited 2024 Jun 27];97(2):466. Available from: /pmc/articles/PMC2112508/?report=abstract

48. Ishihara S, Inman DR, Li WJ, Ponik SM, Keely PJ. Mechano-signal transduction in mesenchymal stem cells induces prosaposin secretion to drive the proliferation of breast cancer cells.

742 49. O'Connell JT, Sugimoto H, Cooke VG, MacDonald BA, Mehta AI, LeBleu VS, et al.
743 VEGF-A and Tenascin-C produced by S100A4 + stromal cells are important for
744 metastatic colonization. Proc Natl Acad Sci U S A [Internet]. 2011 Oct 20 [cited 2024
745 Jun 17];108(38):16002–7. Available from:
746 www.pnas.org/cgi/doi/10.1073/pnas.1109493108

747 50. Kyutoku M, Taniyama Y, Katsuragi N, Shimizu H, Kunugiza Y, Iekushi K, et al. Role of
748 periostin in cancer progression and metastasis: Inhibition of breast cancer
749 progression and metastasis by anti-periostin antibody in a murine model. Int J Mol
750 Med [Internet]. 2011 Aug 1 [cited 2024 Jun 17];28(2):181–6. Available from:
751 http://www.spandidos-publications.com/10.3892/ijmm.2011.712/abstract

752 51. Wang C, Chen YG, Gao JL, Lyu GY, Su J, Zhang Q, et al. Low local blood perfusion,
753 high white blood cell and high platelet count are associated with primary tumor
754 growth and lung metastasis in a 4T1 mouse breast cancer metastasis model. Oncol
755 Lett [Internet]. 2015 Aug 1 [cited 2024 May 13];10(2):754–60. Available from:
756 http://www.spandidos-publications.com/10.3892/ol.2015.3304/abstract

757 52. Barrios M, Rodríguez-Acosta A, Gil A, Salazar AM, Taylor P, Sánchez EE, et al.
758 Comparative hemostatic parameters in BALB/c, C57BL/6 and C3H/He mice. Thromb
759 Res. 2009 Jul 1;124(3):338–43.

760 53. Bendele A, Seely J, Richey C, Sennello G, Shopp G. Short Communication: Renal
761 Tubular Vacuolation in Animals Treated with Polyethylene-Glycol-Conjugated
762 Proteins. 1998 [cited 2024 May 12]; Available from:
763 https://academic.oup.com/toxsci/article/42/2/152/1685757

764 54. Singh P, Carraher C, Schwarzbauer JE. Assembly of Fibronectin Extracellular Matrix.
765 Annu Rev Cell Dev Biol [Internet]. 2010 Nov 10 [cited 2024 May 13];26:397. Available
766 from: /pmc/articles/PMC3628685/

767 55. Harburger DS, Calderwood DA. Integrin signalling at a glance. J Cell Sci [Internet].
768 2009 Jan 1 [cited 2024 May 13];122(2):159. Available from:
769 /pmc/articles/PMC2714413/

770 56. Sun L, Guo S, Xie Y, Yao Y. The characteristics and the multiple functions of integrin
771 β1 in human cancers. J Transl Med [Internet]. 2023 [cited 2024 Jun 18];21:787.
772 Available from: https://doi.org/10.1186/s12967-023-04696-1

773 57. Michael KE, Dumbauld DW, Burns KL, Hanks SK, García AJ. Focal adhesion kinase
774 modulates cell adhesion strengthening via integrin activation. Mol Biol Cell

775 [Internet]. 2009 May 1 [cited 2024 Jun 18];20(9):2508–19. Available from:
776 https://www.molbiolcell.org/doi/10.1091/mbc.e08-01-0076

777 58. Han H jun, Sung JY, Kim SH, Yun UJ, Kim H, Jang EJ, et al. Fibronectin regulates
778 anoikis resistance via cell aggregate formation. Cancer Lett. 2021 Jun 28;508:59–72.

779 59. Haun F, Neumann S, Peintner L, Wieland K, Habicht J, Schwan C, et al. Identification
780 of a novel anoikis signalling pathway using the fungal virulence factor gliotoxin. [cited
781 2024 Jul 15]; Available from: www.nature.com/naturecommunications

782 60. Van Nimwegen MJ, Huigsloot M, Camier A, Tijdens IB, Van De Water B. Focal
783 Adhesion Kinase and Protein Kinase B Cooperate to Suppress Doxorubicin-Induced
784 Apoptosis of Breast Tumor Cells. 2006 [cited 2024 Jul 14]; Available from:
785 http://molpharm.aspetjournals.org.

786 61. Kurenova E, Xu LH, Yang X, Albert S. Baldwin Jr, Craven RJ, Hanks SK, et al. Focal
787 Adhesion Kinase Suppresses Apoptosis by Binding to the Death Domain of Receptor-
788 Interacting Protein. Mol Cell Biol [Internet]. 2004 May 1 [cited 2024 Jul
789 14];24(10):4361. Available from: /pmc/articles/PMC400455/

790 62. Han Z, Lu ZR. Targeting Fibronectin for Cancer Imaging and Therapy. Journal of
791 materials chemistry B, Materials for biology and medicine [Internet]. 2017 [cited
792 2022 May 7];5(4):639. Available from: /pmc/articles/PMC5733799/

793 63. Kumra H, Reinhardt DP. Fibronectin-targeted drug delivery in cancer. Adv Drug Deliv
794 Rev. 2016 Feb 1;97:101–10.

795 64. Frey K, Schliemann C, Schwager K, Giavazzi R, Johannsen M, Neri D. The
796 immunocytokine F8-IL2 improves the therapeutic performance of sunitinib in a
797 mouse model of renal cell carcinoma. Journal of Urology. 2010 Dec;184(6):2540–8.

798 65. Martín-Otal C, Lasarte-Cia A, Serrano D, Casares N, Conde E, Navarro F, et al.
799 Targeting the extra domain A of fibronectin for cancer therapy with CAR-T cells. J
800 Immunother Cancer [Internet]. 2022 Aug 2 [cited 2024 Jun 29];10(8). Available from:
801 https://pubmed.ncbi.nlm.nih.gov/35918123/

802 66. Jiang K, Song X, Yang L, Li L, Wan Z, Sun X, et al. Enhanced antitumor and anti-
803 metastasis efficacy against aggressive breast cancer with a fibronectin-targeting
804 liposomal doxorubicin. Journal of Controlled Release. 2018 Feb 10;271:21–30.

805 67. Oh E, Pierschbacher M, Ruoslahti E. Medical Sciences Deposition of plasma
806 fibronectin in tissues (extracellular matrix/basement membranes/plasma proteins).
807 1981 [cited 2024 May 13];78(5):3218–21. Available from: https://www.pnas.org

68. Lin TC, Yang CH, Cheng LH, Chang WT, Lin YR, Cheng HC. Fibronectin in Cancer: Friend or Foe. Cells [Internet]. 2020 Jan 1 [cited 2024 May 13];9(1). Available from: /pmc/articles/PMC7016990/

69. Giancotti FG, Ruoslahti E. Integrin Signaling. [cited 2024 May 13]; Available from: https://www.science.org

70. Longstreth JH, Wang K. The role of fibronectin in mediating cell migration. Am J Physiol Cell Physiol [Internet]. 2024 Apr 1 [cited 2024 Jun 29];326(4):C1212–25. Available from: https://pubmed.ncbi.nlm.nih.gov/38372136/

71. Oudin MJ, Jonas O, Kosciuk T, Broye LC, Guido BC, Wyckoff J, et al. Tumor cell–driven extracellular matrix remodeling drives haptotaxis during metastatic progression. Cancer Discov [Internet]. 2016 May 1 [cited 2024 Jul 15];6(5):516–31. Available from: /cancerdiscovery/article/6/5/516/5516/Tumor-Cell-Driven-Extracellular-Matrix-Remodeling

72. A small-molecule RGD-integrin antagonist inhibits cell adhesion, cell migration and induces anoikis in glioblastoma cells [Internet]. [cited 2024 May 13]. Available from: https://www.spandidos-publications.com/ijo/42/1/83

73. Winkler J, Abisoye-Ogunniyan A, Metcalf KJ, Werb Z. Concepts of extracellular matrix remodelling in tumour progression and metastasis. Nat Commun [Internet]. 2020 Dec 1 [cited 2023 Aug 15];11(1). Available from: /pmc/articles/PMC7547708/

74. Farrar CS, Hocking DC. Assembly of fibronectin fibrils selectively attenuates platelet-derived growth factor–induced intracellular calcium release in fibroblasts. J Biol Chem [Internet]. 2018 Nov 11 [cited 2024 Jul 14];293(48):18655. Available from: /pmc/articles/PMC6290149/

75. He J, Steffen JH, Thulstrup PW, Pedersen JN, Sauerland MB, Otzen DE, et al. Anastellin impacts on the processing of extracellular matrix fibronectin and stimulates release of cytokines from coronary artery smooth muscle cells. Scientific Reports 2022 12:1 [Internet]. 2022 Dec 21 [cited 2024 Jul 14];12(1):1–15. Available from: https://www.nature.com/articles/s41598-022-26359-9

76. Belitškin D, Pant SM, Munne P, Suleymanova I, Belitškina K, Hongisto H, et al. Hepsin regulates TGFβ signaling via fibronectin proteolysis. EMBO Rep [Internet]. 2021 Nov 11 [cited 2024 Jul 14];22(11). Available from: /pmc/articles/PMC8567232/

77. Wei L, Chen Q, Zheng Y, Nan L, Liao N, Mo S. Potential Role of Integrin α5β1/Focal Adhesion Kinase (FAK) and Actin Cytoskeleton in the Mechanotransduction and Response of Human Gingival Fibroblasts Cultured on a 3-Dimension Lactide-Co-

Glycolide (3D PLGA) Scaffold. Med Sci Monit [Internet]. 2020 Feb 8 [cited 2024 Jul 14];26:e921626-1. Available from: /pmc/articles/PMC7027369/

78. Levkau B, Herren B, Koyama H, Ross R, Raines EW. Caspase-mediated Cleavage of Focal Adhesion Kinase pp125 FAK and Disassembly of Focal Adhesions in Human Endothelial Cell Apoptosis. J Exp Med [Internet]. 1998 [cited 2024 Apr 27];187(4):579–86. Available from: http://www.jem.org

79. Hadden HL, Henke CA. Induction of Lung Fibroblast Apoptosis by Soluble Fibronectin Peptides. https://doi.org/101164/ajrccm16242001015 [Internet]. 2012 Dec 14 [cited 2024 Apr 27];162(4 I):1553–60. Available from: www.atsjournals.org

80. Frisch SM, Vuori K, Ruoslahti E, Chan-Hui Y, Bristol *, Squibb M. Control of Adhesion-dependent Cell Survival by Focal Adhesion Kinase. [cited 2024 Jul 14]; Available from: http://rupress.org/jcb/article-pdf/134/3/793/1480423/793.pdf

81. Gilmore AP, Metcalfe AD, Romer LH, Streuli CH. Integrin-Mediated Survival Signals Regulate the Apoptotic Function of Bax through Its Conformation and Subcellular Localization. Journal of Cell Biology [Internet]. 2000 Apr 17 [cited 2024 Jul 14];149(2):431–46. Available from: http://www.jcb.org

82. Ko Ili DŠ, Almeida EAC, Schlaepfer DD, Dazin P, Aizawa S, Damsky CH, et al. Extracellular Matrix Survival Signals Transduced by Focal Adhesion Kinase Suppress p53-mediated Apoptosis. J Cell Biol [Internet]. 1998 [cited 2024 Jul 14];143(2):547–60. Available from: http://www.jcb.org

83. Kabir J, Lobo M, Zachary I. Staurosporine induces endothelial cell apoptosis via focal adhesion kinase dephosphorylation and focal adhesion disassembly independent of focal adhesion kinase proteolysis. Biochemical Journal [Internet]. 2002 Oct 10 [cited 2024 Jul 14];367(Pt 1):145. Available from: /pmc/articles/PMC1222856/?report=abstract

84. Hazlehurst LA, Argilagos RF, Emmons M, Boulware D, Beam CA, Sullivan DM, et al. Cell Adhesion to Fibronectin (CAM-DR) Influences Acquired Mitoxantrone Resistance in U937 Cells. Cancer Res [Internet]. 2006 [cited 2024 Jul 14];66(4):2338–83. Available from: http://aacrjournals.org/cancerres/article-pdf/66/4/2338/2558035/2338.pdf

85. Ye Y, Zhang R, Feng H. Fibronectin promotes tumor cells growth and drugs resistance through a CDC42-YAP-dependent signaling pathway in colorectal cancer. Cell Biol Int [Internet]. 2020 Sep 1 [cited 2024 Jul 14];44(9):1840–9. Available from: https://onlinelibrary.wiley.com/doi/full/10.1002/cbin.11390

86. Nakagawa Y, Nakayama H, Nagata M, Yoshida R, Kawahara K, Hirosue A, et al. Overexpression of fibronectin confers cell adhesion-mediated drug resistance (CAM-DR) against 5-FU in oral squamous cell carcinoma cells. Int J Oncol [Internet]. 2014 Apr [cited 2024 Jul 14];44(4):1376–84. Available from: https://pubmed.ncbi.nlm.nih.gov/24452447/

87. Polydorou C, Mpekris F, Papageorgis P, Voutouri C, Stylianopoulos T. Pirfenidone normalizes the tumor microenvironment to improve chemotherapy. 2017 [cited 2023 Jul 24];8(15):24506–17. Available from: www.impactjournals.com/oncotarget